
DRAFT

CMS Paper

The content of this note is intended for CMS internal use and distribution only

2009/08/17

Archive Id: 1.5

Archive Date: 2009/08/17 21:14:15

Measurement of the Dijet Mass Distribution and Search for New Particles in pp Collisions at 10 TeV

The CMS Collaboration

Abstract

We present an early paper draft, which contains only simulation and theory, but what follows is written as if it were reporting a real measurement of early CMS data.

We have used 10 pb^{-1} of integrated luminosity from the CMS experiment at the Large Hadron Collider at CERN to search for new particles decaying to dijets. The measured dijet mass spectrum agrees with QCD predictions. We exclude at the 95% confidence level models containing the following new particles: axiguons and flavor universal colorons with mass below $1.8 \text{ TeV}/c^2$, excited quarks with mass below $1.8 \text{ TeV}/c^2$ and E_6 diquarks with mass below $1.0 \text{ TeV}/c^2$ and within the range $1.3\text{--}1.7 \text{ TeV}/c^2$.

This box is only visible in draft mode. Please make sure the values below make sense.

PDFAuthor:	Robert Harris, Chiyoung Jeong, Kostas Kousouris, Sung-Won Lee, Sertac Ozturk
PDFTitle:	Measurement of the Dijet Mass Distribution and Search for New Particles in pp Collisions at 10 TeV
PDFSubject:	CMS
PDFKeywords:	CMS, physics, software, computing

Please also verify that the abstract does not use any user defined symbols

1 Within the standard model events with two energetic jets (dijets) are expected to arise in proton-
 2 proton collisions from parton-parton scattering. The outgoing scattered partons manifest them-
 3 selves as hadronic jets. The dijet mass spectrum predicted by Quantum Chromodynamics
 4 (QCD) falls smoothly and steeply with increasing dijet mass. Many extensions of the stan-
 5 dard model predict the existence of new massive objects that couple to quarks (q) and gluons
 6 (g), and result in resonant structures in the dijet mass spectrum. In this paper we report a search
 7 for narrow resonances in the dijet mass spectrum, measured with the Compact Muon Solenoid
 8 (CMS) detector at the CERN Large Hadron Collider, at a proton-proton collision energy of
 9 $\sqrt{s} = 10$ TeV.

10 In addition to this generic search, we specifically search for the following seven models of dijet
 11 resonances. First, in a model where the symmetry group $SU(3)$ of QCD is replaced by the
 12 chiral symmetry $SU(3)_L \times SU(3)_R$, there are axial vector particles called axigluons A which
 13 decay to $q\bar{q}$ [1]. Second, the flavor-universal coloron model also embeds the $SU(3)$ of QCD in a
 14 larger gauge group, and predicts the presence of a color-octet coloron C which decays to $q\bar{q}$ [2].
 15 Third, if quarks are composite particles then excited states are expected, and we search for mass
 16 degenerate excited quarks q^* that decay to qg [3]. Fourth, grand unified theory based on the E_6
 17 gauge group predicts the presence of scalar diquarks D and D^c which decay to $\bar{q}\bar{q}$ and qq [4].
 18 Fifth, the Randall-Sundrum model of extra dimensions predicts massive gravitons G which
 19 decay to $q\bar{q}$ and gg [5]. Sixth and Seventh, models which propose new gauge symmetries often
 20 predict new gauge bosons W' and Z' which decay to $q\bar{q}$ [6].

21 A detailed description of the CMS experiment can be found elsewhere [7, 8]. The CMS coordi-
 22 nate system has the origin at the center of the detector, z -axis points along the beam direction
 23 toward the west, with the transverse plane perpendicular to the beam. We define ϕ to be the
 24 azimuthal angle, θ to be the polar angle and the pseudorapidity as $\eta \equiv -\ln(\tan[\theta/2])$. The
 25 central feature of the CMS apparatus is a superconducting solenoid, of 6 m internal diame-
 26 ter. Within the field volume are the silicon pixel and strip tracker, and the barrel and endcap
 27 calorimeters ($|\eta| < 3$): a crystal electromagnetic calorimeter (ECAL) and a brass-scintillator
 28 hadronic calorimeter (HCAL). Outside the field volume, in the forward region, there is an iron-
 29 quartz fiber hadronic calorimeter ($3 < |\eta| < 5$). The HCAL and ECAL cells are grouped into
 30 towers, projecting radially outward from the origin, for triggering purposes and to facilitate
 31 the jet reconstruction. In the region $|\eta| < 1.74$ these projective calorimeter towers have seg-
 32 mentation $\Delta\eta = \Delta\phi = 0.087$, and the η and ϕ width progressively increases at higher values
 33 of η . The energy in the HCAL and ECAL within each projective tower is summed to find the
 34 calorimeter tower energy. Towers with $|\eta| < 1.3$ contain only cells from the barrel calorimeters,
 35 towers in the transition region $1.3 < |\eta| < 1.5$ contain a mixture of barrel and endcap cells, and
 36 towers in the region $1.5 < |\eta| < 3.0$ contain only cells from the endcap calorimeters.

37 Jets are reconstructed using the seedless infrared safe cone algorithm with cone size $R =$
 38 $\sqrt{(\Delta\eta)^2 + (\Delta\phi)^2} = 0.7$ [9]. Below we will discuss three types of jets: reconstructed, corrected
 39 and generated. The reconstructed jet energy, E , is defined as the scalar sum of the calori-
 40 meter tower energies inside the jet. The jet momentum, \vec{p} , is the corresponding vector sum:
 41 $\vec{p} = \sum E_i \hat{u}_i$ with \hat{u}_i being the unit vector pointing from the origin to the energy deposition E_i
 42 inside the cone. The jet transverse momentum, p_T , is the component of \vec{p} in the transverse
 43 plane. The E and \vec{p} of a reconstructed jet are then corrected for the non-linear response of the
 44 calorimeter to a generated jet. Generated jets come from applying the same jet algorithm to the
 45 Lorentz vectors of stable generated particles before detector simulation. On average, the p_T
 46 of a corrected jet is equal to the p_T of the corresponding generated jet. The corrections estimated
 47 from a GEANT [10] simulation of the CMS detector increase the average jet p_T by roughly 50%
 48 (10%) for 70 GeV (3 TeV) jets in the region $|\eta| < 1.3$. Further details on jet reconstruction and jet

energy corrections can be found elsewhere [11, 12]. The jet measurements presented here are within the region $|\eta| < 1.3$, where the sensitivity to new physics is expected to be the highest, and where the reconstructed jet response variations as a function of η are both moderate and smooth.

The dijet system is composed of the two jets with the highest p_T in an event (leading jets), and the dijet mass is given by $m = \sqrt{(E_1 + E_2)^2 - (\vec{p}_1 + \vec{p}_2)^2}$. We require both leading jets have pseudorapidity $|\eta| < 1.3$. The estimated dijet mass resolution varies from 9% at a dijet mass of 0.7 TeV to 4.5% at 5 TeV. We use data from the 2009-2010 running period corresponding to an integrated luminosity of 10 pb^{-1} . The sample we use for this search was collected by requiring at least one jet in the high level trigger with $p_T > 110 \text{ GeV}/c$. The trigger efficiency, measured from a sample acquired with a prescaled trigger with a lower p_T threshold, was greater than 99% for dijet mass above $420 \text{ GeV}/c^2$. Backgrounds from cosmic rays, beam halo, and detector noise are expected to occasionally produce events with large or unbalanced energy depositions. They are removed by requiring $\cancel{E}_T / \sum E_T < 0.3$ and $\sum E_T < 10 \text{ TeV}$, where \cancel{E}_T ($\sum E_T$) is the magnitude of the vector (scalar) sum of the transverse energies measured by all calorimeter towers in the event. This cut is more than 99% efficient for both QCD jet events and the signals of new physics considered. In the high p_T region relevant for this search, jet reconstruction is fully efficient.

In Fig. 1 we present the inclusive dijet mass distribution for $p\bar{p} \rightarrow 2 \text{ leading jets} + X$, where X can be anything including additional jets. We plot the differential cross section versus dijet mass in bins approximately equal to the dijet mass resolution. The systematic uncertainty on the cross section arises predominantly from a 10% uncertainty on the jet energy correction, but also includes a 10% uncertainty on the luminosity. The data is compared to a prediction from PYTHIA [13] which includes a simulation of the CMS detector and the jet energy corrections. The data is also compared with a full QCD prediction at next-to-lowest order [14]. Both predictions use CTEQ6 parton distributions [15] and a renormalization scale $\mu = p_T$. The data agrees with both predictions within the systematic uncertainties of the measurement. To test the smoothness of our measurement as a function of dijet mass, we fit the data with the parameterization

$$\frac{d\sigma}{dm} = \frac{P0[1 - (m/\sqrt{s}) + P3(m/\sqrt{s})^2]^{P1}}{m^{P2}} \quad (1)$$

with the four parameters $P0$, $P1$, $P2$ and $P3$. In Fig. 2 we show both the data and the background fit, which has a χ^2 of 23 for 32 degrees of freedom. In Fig. 3 we show the fractional difference between the data and the background fit. The data is well fit by the smooth parameterization and shows no evidence of new particles.

To set limits on dijet resonances we require a model of the resonance line shape. In Fig. 2 and 3 we show the predicted line shape for excited quarks (q^*) using the PYTHIA Monte Carlo [13] and a CMS detector simulation. The mass resolution has a Gaussian core from jet energy resolution and a long tail towards low mass from QCD radiation. The line shape of narrow dijet resonances depends on the type of partons involved in the resonance, because this affects both the amount of radiation and also the final state jet response in the CMS detector. In Fig. 4 we show examples of the predicted line shape of dijet resonances from three different parton pairings: $q\bar{q}$ resonances found from the process $q\bar{q} \rightarrow G \rightarrow q\bar{q}$, qg resonances found from the process $qg \rightarrow q^* \rightarrow qg$, and gg resonances found from the process $gg \rightarrow G \rightarrow gg$. The width of dijet resonances increases with the number of gluons in the $2 \rightarrow 2$ process, primarily because gluons emit more radiation than quarks. The peak value of dijet mass of the resonance decreases with the number of final state gluons, primarily due to smaller response of the CMS detector to gluons than to quarks. These resonance shapes are approximately valid for any

84 model of resonance involving these pairs of partons assuming the models natural half-width
85 ($\Gamma/2$) is small compared to the dijet mass resolution.

86 We use the dijet resonance shapes to set separate limits on new particles decaying to the parton
87 pairs qq (or $q\bar{q}$), qg and gg . We perform a binned maximum likelihood fit of the data to both the
88 background parameterization and the signal hypothesis. The method gave a Poisson likelihood
89 as a function of the signal cross section. This was done independently at 29 different values of
90 new particle mass from 0.7 to 3.5 TeV/c^2 in 0.1 TeV/c^2 steps resulting in 29 statistical likeli-
91 hood distributions from which we found initial 95% confidence level upper limits on the cross
92 section including only statistical uncertainties. Including a 10% systematic uncertainty in the
93 measured dijet mass gave an uncertainty in the limit which varied from 43% at 0.7 to 28% at 3.5
94 TeV/c^2 . The cross section limit also depended on the choice of background parameterization,
95 varying from 8% at 0.7 to 40% at 3.5 TeV/c^2 . The systematic uncertainty on the integrated lu-
96 minosity was 10%. We combined these uncertainties in quadrature and convoluted each of the
97 29 Poisson likelihoods with the Gaussian systematic uncertainty and found the final 95% con-
98 fidence level upper limits on the cross section presented in Table 1. The systmatic uncertainties
99 increased the limit by roughly 50%.

100 In Fig. 5 we compare our measured upper limit on the cross section times branching ratio
101 for a new particle decaying to dijets to the theoretical predictions. The predictions are lowest
102 order calculations with CTEQ6L parton distributions [15] for dijets with $|\eta| < 1.3$. We exclude
103 at 95% C.L. new particles in mass regions for which the theory curve lies above our upper
104 limit for the appropriate pair of partons. For axigluons (or flavor universal colorons) we use
105 our limits on qq resonances to exclude the mass range $0.7 < M(A) < 1.8 \text{ TeV}/c^2$, extending
106 the previous exclusions [16] of $120 < M(A) < 1250 \text{ GeV}/c^2$. For excited quarks we use our
107 limits on qg resonances to exclude the mass range $0.7 < M(q^*) < 1.8 \text{ TeV}/c^2$, extending the
108 previous exclusions [16] of $260 < M(q^*) < 870 \text{ GeV}/c^2$. For E_6 diquarks we use our limits on
109 qq resonances to exclude the mass range $0.7 < M(D) < 1.0 \text{ TeV}/c^2$, and $1.3 < M(D) < 1.7$
110 TeV/c^2 , extending the previous exclusions [16] of $290 < M(D) < 630 \text{ GeV}/c^2$. The systematic
111 uncertainties in this analysis reduced the highest excluded mass by roughly 0.1 TeV/c^2 for each
112 type of new particle.

113 In conclusion, the measured dijet mass spectrum is a smoothly falling distribution which agrees
114 with the predictions of the standard model. We see no significant evidence for new particle pro-
115 duction and set limits on axigluons, flavor universal colorons, excited quarks, and E_6 diquarks.

116 We thank the technical and administrative staffs at CERN and other CMS Institutes, and ac-
117 knowledge support from: FMSR (Austria); FNRS and FWO (Belgium); CNPq and FAPERJ
118 (Brazil); MES (Bulgaria); CERN; CAS and NSFC (China); MST (Croatia); University of Cyprus
119 (Cyprus); Academy of Sciences and NICPB (Estonia); Academy of Finland, ME and HIP (Fin-
120 land); CEA and CNRS/IN2P3 (France); BMBF and DESY (Germany); GSRT (Greece); NKTH
121 (Hungary); DAE and DST (India); IPM (Iran); UCD (Ireland); INFN (Italy); KICOS (Korea);
122 CINVESTAV, CONACYT and UASLP-FAI (Mexico); PAEC (Pakistan); SCSR (Poland); FCT
123 (Portugal); JINR (Armenia, Belarus, Georgia, Ukraine, Uzbekistan); MST and MAE (Russia);
124 MSEP (Serbia); OCT (Spain); ETHZ, PSI, University of Zurich (Switzerland); NSC (Taipei);
125 TUBITAK and TAEK (Turkey); STFC (United Kingdom); DOE and NSF (USA).

126 References

127 [1] P. H. Frampton and S. L. Glashow *Phys. Lett.* **B190** (1987) 157.

- 128 [2] E. H. Simmons *Phys. Rev.* **D55** (1997) 1678.
- 129 [3] U. Baur, I. Hinchliffe, and D. Zeppenfeld *Int. J. Mod. Phys.* **A2** (1987) 1285.
- 130 [4] J. L. Hewett and T. G. Rizzo *Phys. Rept.* **183** (1989) 193.
- 131 [5] L. Randall and R. Sundrum *Phys. Rev. Lett.* **83** (1999) 4690.
- 132 [6] E. Eichten, I. Hinchliffe, K. D. Lane, and C. Quigg *Rev. Mod. Phys.* **56** (1984) 579.
- 133 [7] **CMS** Collaboration, R. Adolphi et al. *JINST* **0803** (2008) S08004.
- 134 [8] **CMS** Collaboration, G. L. Bayatian et al. CERN-LHCC-2006-001.
- 135 [9] G. P. Salam and G. Soyez *JHEP* **05** (2007) 086.
- 136 [10] **GEANT4** Collaboration, S. Agostinelli et al. *Nucl. Instrum. Meth.* **A506** (2003) 250.
- 137 [11] **CMS** Collaboration *CMS Physics Analysis Summary* **JME-07-002** (2008).
- 138 [12] **CMS** Collaboration *CMS Physics Analysis Summary* **JME-07-003** (2008).
- 139 [13] T. Sjostrand, L. Lonnblad, and S. Mrenna [arXiv:hep-ph/0108264](https://arxiv.org/abs/hep-ph/0108264).
- 140 [14] Z. Nagy *Phys. Rev.* **D68** (2003) 094002.
- 141 [15] J. Pumplin et al. *JHEP* **07** (2002) 012.
- 142 [16] **CDF** Collaboration, T. Aaltonen et al. *Phys. Rev.* **D79** (2009) 112002.

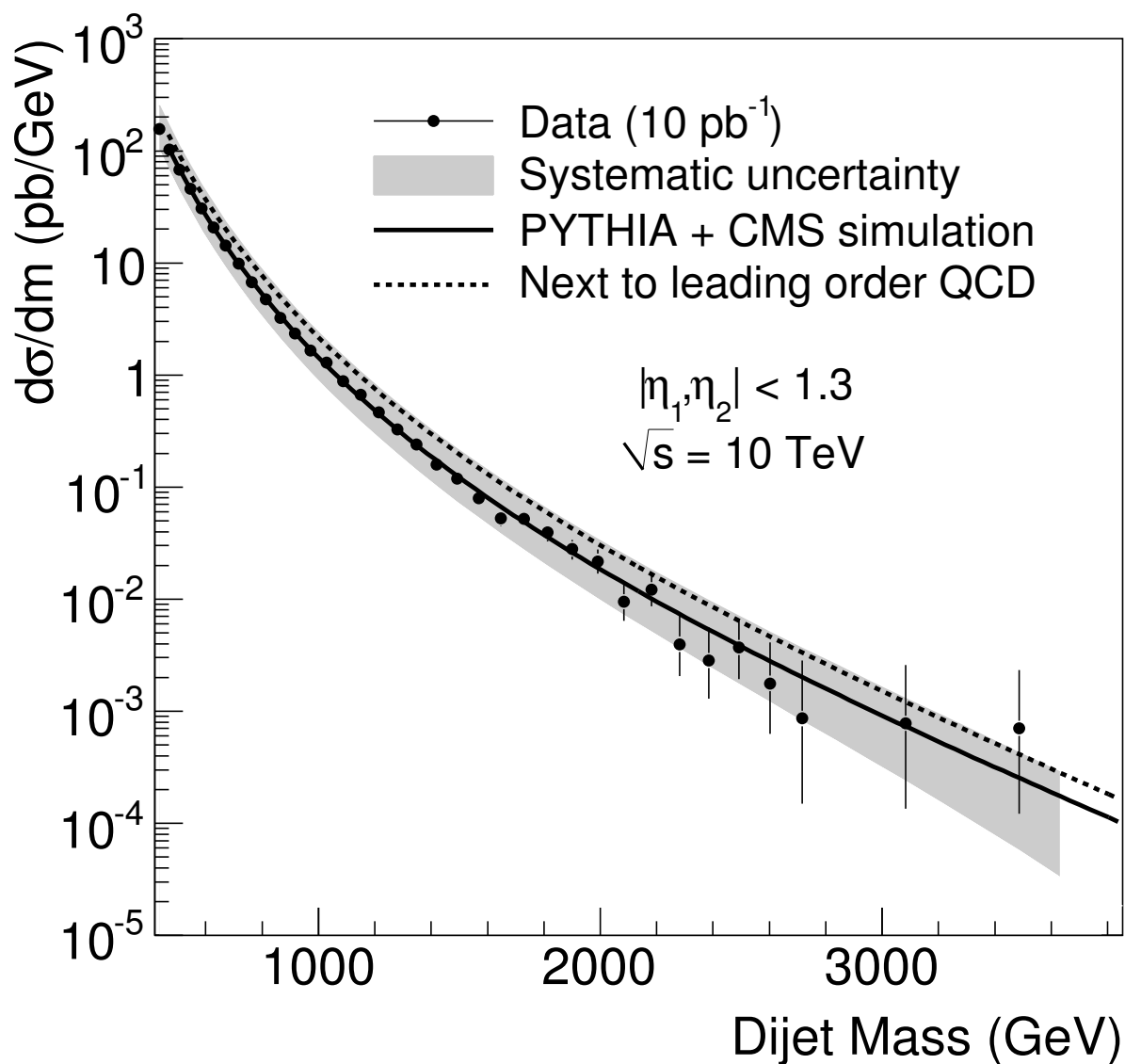


Figure 1: The dijet mass distribution (points) compared to a simulation of QCD and the CMS detector (solid curve) and a next-to-leading order QCD calculation (dashed curve). The band shows the systematic uncertainties on the data. WARNING: CMS DATA IN THIS FIGURE IS FAKE

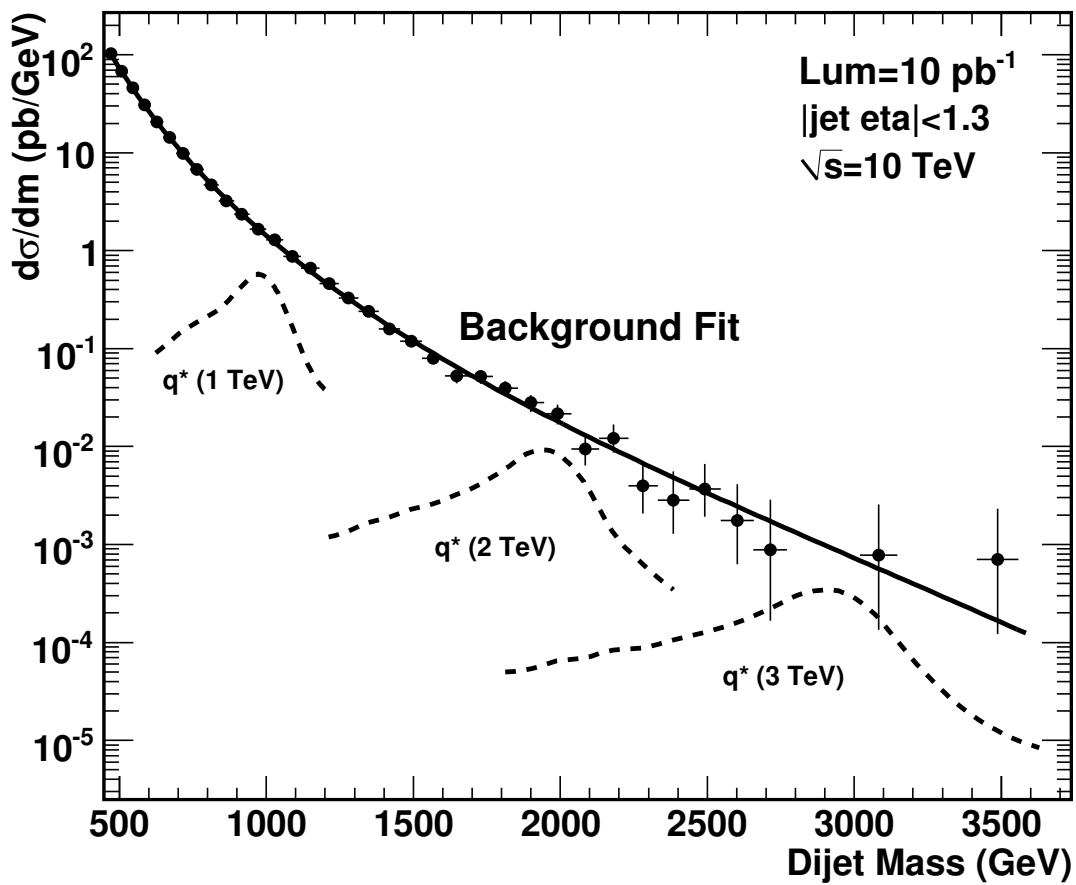


Figure 2: The dijet mass distribution (points) compared to a smooth background fit (solid curve) and to a simulation of excited quarks signals in the CMS detector (dashed curves).
WARNING: CMS DATA IN THIS FIGURE IS FAKE

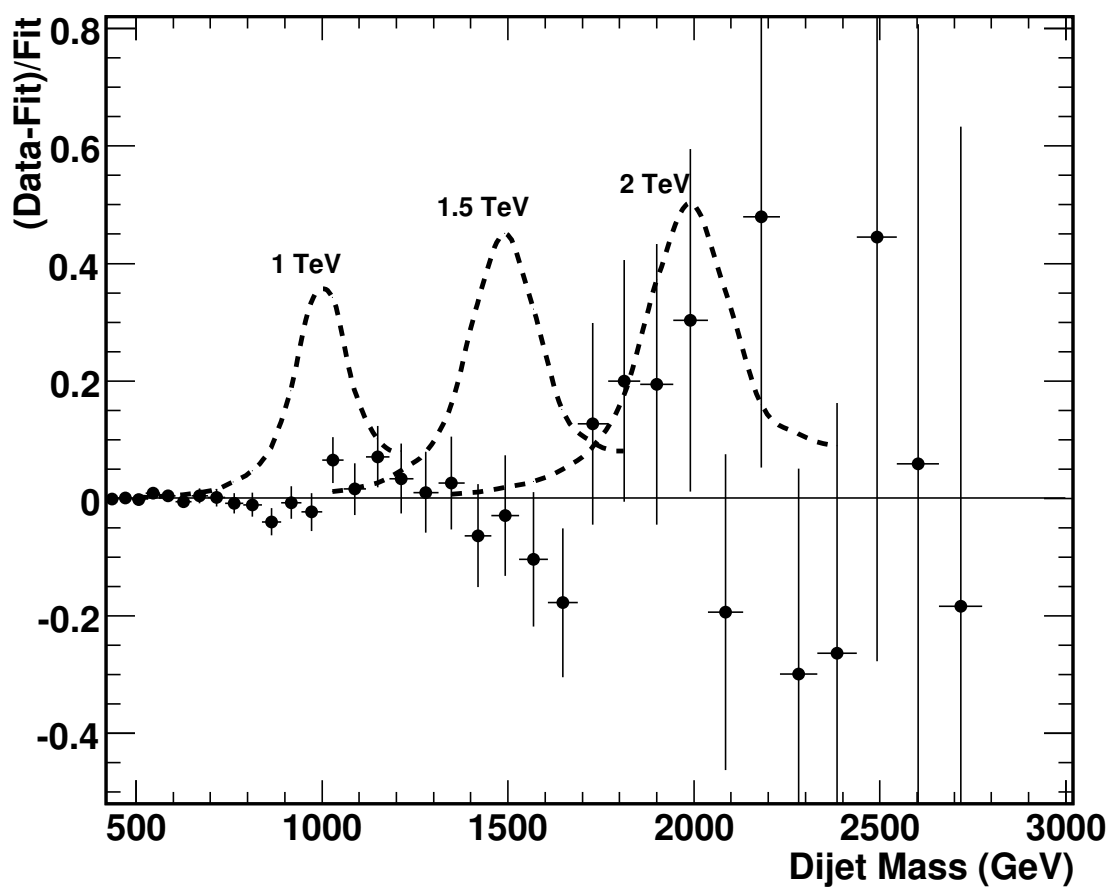


Figure 3: The fractional difference between the dijet mass distribution (points) and a smooth background fit (solid line) is compared to simulations of excited quark signals in the CMS detector (dashed curves). WARNING: CMS DATA IN THIS FIGURE IS FAKE

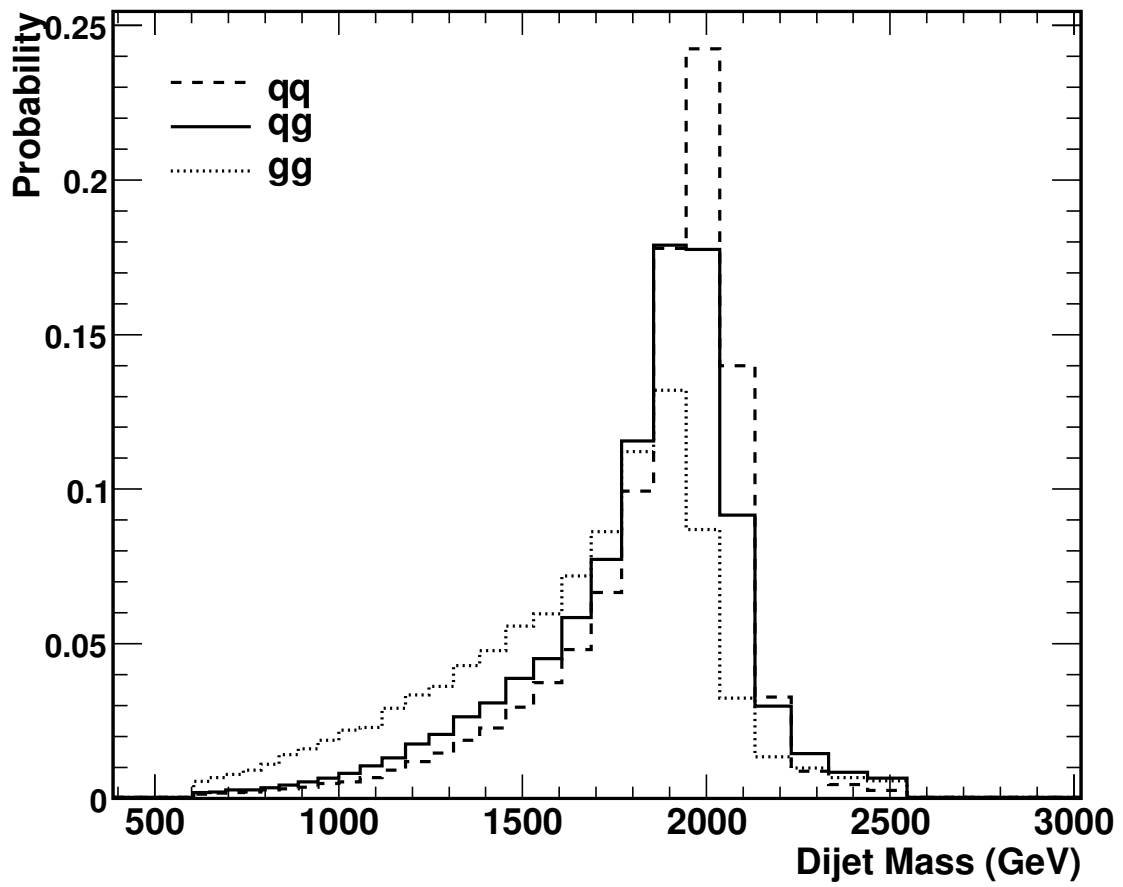


Figure 4: Simulations of the dijet mass distribution for narrow resonances with mass 2 TeV involving parton pairs of type quark-quark (dashed), quark-gluon (solid), and gluon-gluon (dotted).

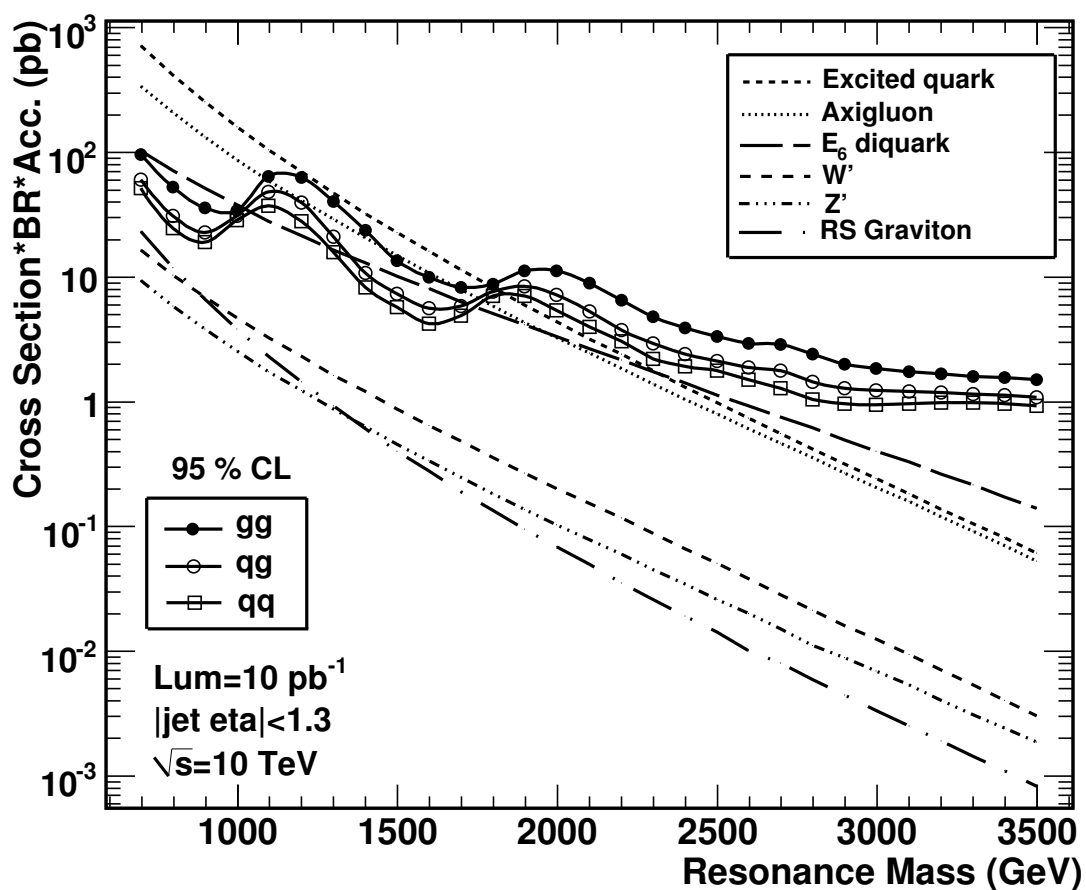


Figure 5: The upper limit on the cross section times branching ratio for new particles decaying to dijets with partons of type gluon-gluon (solid circles), quark-gluon (open circles), and quark-quark (open boxes) are compared to theoretical predictions for axigluons [1], flavor universal colorons [2], excited quarks [3], E_6 diquarks [4], Randall-Sundrum gravitons [5], and new gauge bosons W' and Z' [6]. The limit and theory curves require that both jets have pseudorapidity $|\eta| < 1.3$. WARNING: FROM FAKE DATA

Table 1: As a function of new particle mass we list our 95% C.L. upper limit on cross section times branching ratio for narrow resonances decaying to dijets with partons of type quark-quark (qq), quark-gluon (qg), and gluon-gluon (gg). The limit applies to the kinematic range where both jets have pseudorapidity $|\eta| < 1.3$ WARNING: FROM FAKE DATA.

Mass (TeV/ c^2)	95% C.L. $\sigma \cdot B$ (pb)		
	qq	qg	gg
0.7	51	60	95
0.8	25	31	52
0.9	19	23	35
1.0	28	31	34
1.1	37	48	64
1.2	28	39	63
1.3	16	21	40
1.4	8.3	11	23
1.5	5.7	7.3	14
1.6	4.2	5.6	9.9
1.7	4.9	5.8	8.3
1.8	6.9	7.6	8.8
1.9	7.1	8.4	11
2.0	5.4	7.2	11
2.1	4.0	5.3	9.0
2.2	3.0	3.7	6.4
2.3	2.2	2.9	4.8
2.4	1.9	2.4	3.9
2.5	1.8	2.1	3.3
2.6	1.5	1.9	2.9
2.7	1.3	1.8	2.9
2.8	1.0	1.5	2.4
2.9	0.95	1.3	2.0
3.0	0.94	1.2	1.8
3.1	0.95	1.2	1.7
3.2	0.97	1.2	1.6
3.3	0.97	1.2	1.6
3.4	0.95	1.1	1.5
3.5	0.92	1.1	1.5